



ORIGINAL ARTICLE

Novel self assembled magnetic Prussian blue graphene based aerogel for highly selective removal of radioactive cesium in water



Humaira Seema

Institute of Chemical Sciences, University of Peshawar, Peshawar 25120, Pakistan

Received 1 July 2019; accepted 21 August 2019

Available online 9 September 2019

KEYWORDS

Magnetic;
Prussian blue;
Graphene;
Self assembly;
Cesium removal

Abstract A novel self-assembled Magnetic Prussian Blue/Reduced Graphene Oxide (3D-MPBRGO) aerogel was prepared by an easy and cost effective process for elimination of radioactive Cesium from contaminated aqueous solution selectively. The 3D-MPBRGO displayed excellent adsorption capability of 3.64 mmol per g or (484.12 mg/g) for Cs (initial 50 mM cesium concentration, pH 7 and 30 °C) and quick separation from solution by applying magnetic field as compared to previously published results for graphene based adsorbents. This excellent removal efficiency of nanocomposite can be ascribed to enlarged adsorbent surface area (402.68 m²/g) and uniform distribution of nanoparticles on RGO which removes aggregation of sheets as well. The thermodynamic analysis displayed exothermic and spontaneous nature of Cs ion adsorption. The experimental data of adsorption isotherm followed the Langmuir isotherm model than that of Tempkin and Freundlich while adsorption kinetics followed pseudo second order.

© 2019 Production and hosting by Elsevier B.V. on behalf of King Saud University. This is an open access article under the CC BY-NC-ND license (<http://creativecommons.org/licenses/by-nc-nd/4.0/>).

1. Introduction

Highly selective removal of Cesium (Cs) is critical for environmental remediation. Since the nuclear weapon's testing in 1950s and 1960s and subsequent nuclear power plants mishaps such as Chernobyl and Fukushima disaster in 1986 and 2011 respectively has resulted into the release of radioactive Cs into our environment. In Pakistan radioactive Cesium created from

nuclear testing, has been usually used for collecting the information regarding soil erosion in agricultural areas, and deposition of sediments in lakes as well. Concerns associated with radio-isotopes of Cesium (Cs-137 and Cs-134 with 30 and 2.06-years half-life) and its main focus on the Cs-137 due to its long half-life, gamma emission, its solubility and mobility in environment along with its selectivity toward the biological systems led to thyroid cancer. Therefore, one of the most important tasks towards environmental remediation is the removal of radioactive Cs from a specifically effected polluted environment. Over the past years numerous studies have been conducted to find more effective and sustainable treatment methods for the removal of Cs from nuclear waste effluents (Liu et al., 2014).

E-mail address: humaira@uop.edu.pk

Peer review under responsibility of King Saud University.



Production and hosting by Elsevier

<https://doi.org/10.1016/j.arabjc.2019.08.009>

1878-5352 © 2019 Production and hosting by Elsevier B.V. on behalf of King Saud University.

This is an open access article under the CC BY-NC-ND license (<http://creativecommons.org/licenses/by-nc-nd/4.0/>).

In recent times, due to strong affinity for Cs ions Prussian Blue (PB, ferric hexacyanoferrate) has fascinated importance due to tremendous removal ability for radioactive Cs ion (Torad *et al.*, 2012). However, after Cs ion sorption, it is hard to separate it from water due to its ultra-fine powder. Although, magnetic separation is a convenient method to recover adsorbent from wastewater but the magnetic nanomaterials are easily aggregated due to magnetism and large active surface. However, anchoring magnetic nanoparticles onto matrix and surface coating is an efficient strategy to improve the stability and expand their application (Yantasee *et al.*, 2007; Yavuz *et al.*, 2006; Sun *et al.*, 2011). Graphene oxide (GO), which is hydrophilic, non-conductive, non-toxic, biodegradable, is able to eliminate radioactive nuclides from contaminated water (Romanchuk *et al.*, 2013). Thus, immobilizing magnetic nanoparticles onto large surface area of GO have potential applications (Cong *et al.*, 2010; Zhang *et al.*, 2013). Recently, Yang *et al.* reported the synthesis of magnetic PB/GO nanocomposites but it is still a great challenge to use this method for a large scale water treatment (Yang *et al.*, 2014).

This research study hopes to find a less expensive and easier way for the elimination of radioactive Cs from nuclear waste effluents by demonstrating an ability of the self-assembled magnetic prussian blue reduced graphene oxide (3D-MPBRGO) aerogel to effectively and selectively filter Cs radionuclide from contaminated water.

The 3D-MPBRGO aerogel was analyzed by different characterization techniques such as X-ray diffraction (XRD), Fourier-transform infrared spectroscopy (FT-IR), high-resolution transmission electron microscopy (HR-TEM), scanning electron microscopy with energy dispersive X-ray spectroscopy (SEM-EDX), Brunauer Emmett and Teller (BET)

surface area analysis, X-ray photoelectron spectroscopy (XPS), magnetic property measurement system (MPMS) analysis. Uniform distribution of magnetite and PB over RGO resulted in separation of sheets in self-assembled structure which eventually lead to increase in selective cesium elimination. The nanomaterial used for Cs⁺ adsorption experiments under different experimental parameters i.e. temperature, pH, initial cesium concentration and contact time while kinetic, thermodynamics and isotherm models were utilized to investigate the experimental results.

2. Experimental

2.1. Materials

All analytical grade chemicals were used. Cesium nitrate, iron chloride (FeCl₃), ethanol potassium ferricyanide and L-Ascorbic acid. GO was synthesized according to the method published in previous work (Seema *et al.*, 2014).

2.2. Synthesis of 3D-MPBRGO aerogel

The 3D-MPBRGO nanocomposite was synthesized as illustrated in Fig. 1.

Modified Massart method was used to prepare magnetite (Fe₃O₄) nanoparticles (Massart, 1981). The aerogel nanocomposite with 1:1 mass ratio of graphene to Prussian blue was prepared as follows. 0.098 g of potassium ferricyanide was added to already sonicated 5 mL of GO aqueous solution (12 mg mL⁻¹) containing magnetite (0.3 g) and sonicated for 1 h again to prepare uniform solution. Then aqueous solution of FeCl₃ (0.032 g in 5 mL) added, followed by 0.6 g L-ascorbic

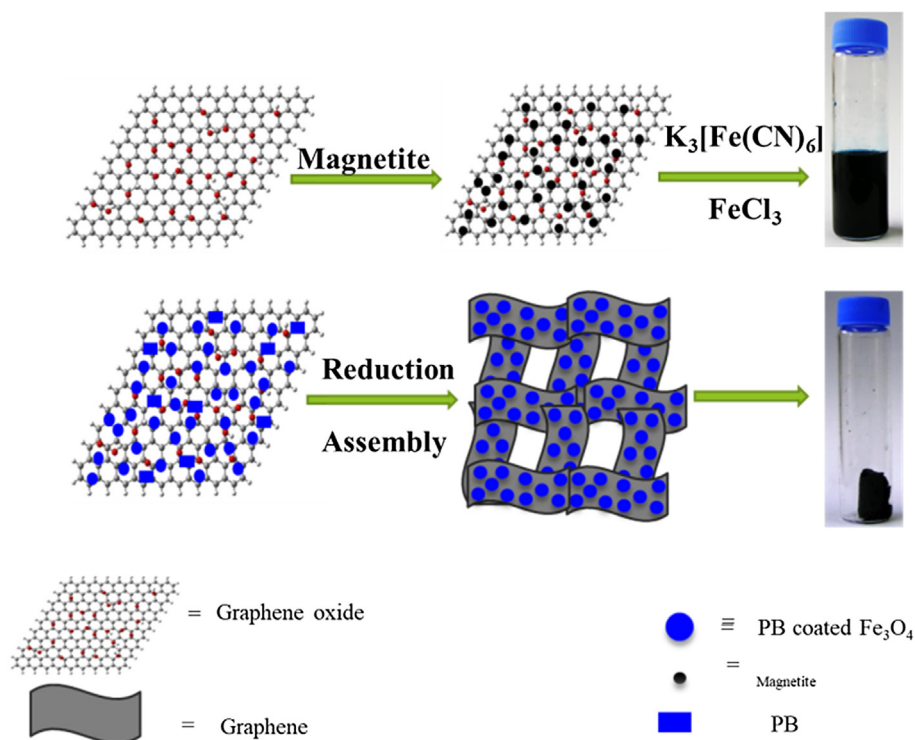


Fig. 1 Synthesis of 3D-MPBRGO aerogel.

acid. After stirring and sonication for 20 min, kept at 40 °C for 12 h to form 3D-MGPBRGO hydrogel. The obtained hydrogel was solvent-exchanged with ethanol to remove all contaminations which includes L-ascorbic acid and its oxidized product. At the last the hydrogel was freeze-dried and grounded for use in adsorption process.

2.3. Characterization for 3D-MPBRGO aerogel

FE-SEM, (S-4800 HITACHI) used for morphology of 3D-MPBRGO aerogel. XRD (RIGAKU, D-2500) with Cu-K α radiation (1.540×10^{-10} m) and FT-IR (Perkin Elmer) were utilized for XRD and IR analysis of aerogel. The attraction capability of aerogel by magnet was investigated by magnetometer (SQUID-VSM QM02) with an applied magnetic strength (-15,000 and 15,000 Oe). TGA (TA Instrument, Q600) used for TGA analysis over a range of certain temperature (till 800 °C from room temperature at specific 10 °C/min heating rate) in the atmosphere of N₂. The surface elemental composition of the 3D-MPBRGO aerogel was investigated via XPS (SXM). FE-HRTEM with Cs probe, used for high resolution structural morphology. BELSORP-max (BEL, JAPAN) was utilized for analysis of surface area analysis.

2.4. Adsorption experiment

The batch method was used to carry out adsorption experiments. In a descriptive procedure, 3D-MPBRGO aerogel (0.03 g) added to CsNO₃ solution (15 mL of 20 mmol) at neutral pH (7.0). The solution containing aerogel was shaken for 24 h at 140 rpm in a shaker at definite temperature (30 °C). By using magnet the adsorbent was removed after adsorption. The mixture was filtered via a syringe filter membrane of 0.22 μ m and Inductively Coupled Plasma Atomic Emission Spectroscopy (ICP-OES) of Perkin Elmer was utilized for Cs determination in the filtrate. The average of three readings for each sample was taken to check adsorption. The following Eq. (1) used for adsorption capacity.

$$q_e = \frac{(C_0 - C_e)V}{W} \quad (1)$$

where q_e (mg/g) is adsorption capacity, C_0 and C_e are cesium concentrations (mmol) initially and at equilibrium, respectively, V (L) is volume of solution while W (g) is weight of adsorbent.

The % R (removal) for cesium by using 3D-MPBRGO aerogel as adsorbent calculated by following Eq. (2)

$$R(\%) = \frac{(C_0 - C_e) \times 100}{C_0} \quad (2)$$

Adsorption kinetics of Cs ion on aerogel was studied by considering Cesium solution (50 mL of 20 mmol) and adsorbent (0.03 g). Samples were taken at specific interval from this solution for determination of adsorption. Adsorption isotherms were studied by addition of 0.03 g adsorbent with Cs⁺ solutions having different concentrations (1–90 mmol). The solution containing adsorbent stirred in shaking incubators for 24 h, 30 °C and 140 rpm. Altered temperatures (e.g. 10–30 °C) were investigated to check the thermodynamic parameters for adsorption process. The HNO₃ (0.1 N) and NaOH (0.1 N) were added to regulate solutions pH (pH = 2–9). The competing ion effect was checked by adding adsorbent to an enriched seawater (50 mL) with MgCl₂ (0.19 g) and NaCl (1.36 g) at different initial Cs⁺ concentrations and shaken constantly for 24 h at 140 rpm. Pseudo first and second order kinetic models used to study the mechanism of Cs⁺ sorption kinetics.

3. Results and discussion

3.1. Characterizations

Fig. 2a shows XRD pattern for the 3D-MPBRGO nanomaterial in which diffraction peaks can be assigned to pure cubic spinel crystals of magnetite of JCPDS card no. 19-0629 and to JCPDS card no. 52-1907 of Prussian blue (Yang et al., 2014). Due to small amount of RGO the characteristic peaks

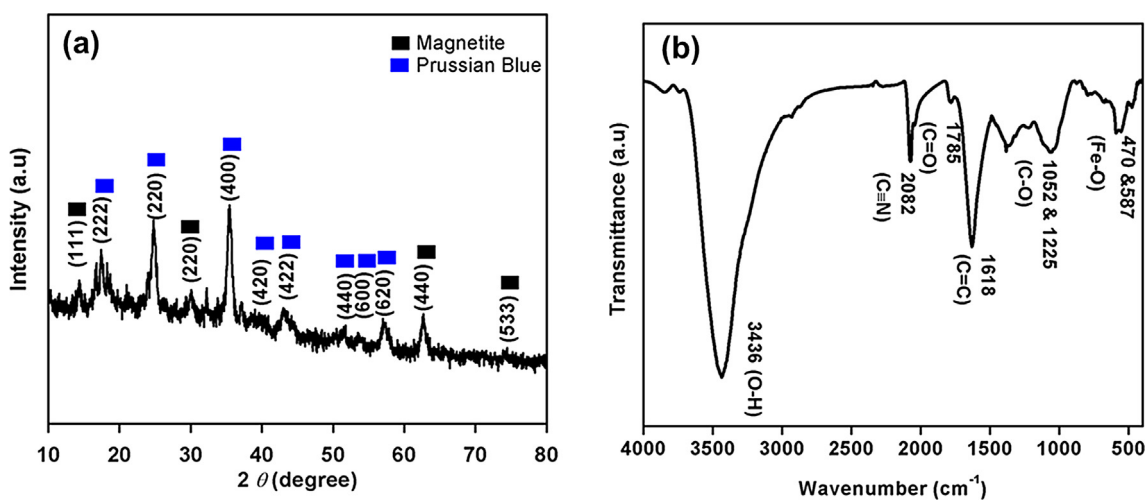


Fig. 2 (a) XRD and, (b) IR of 3D-MPBRGO aerogel.

could not be observed as extremely low XRD detection limit. The FTIR analysis (Fig. 2b) displayed blue shift of absorption peak at 587 from 570 cm^{-1} (Fe—O bond) attributed to size reduction of magnetite to nanoscale dimension. The other absorption peaks of C—O (1052 and 1225 cm^{-1}), —C=O (1785 cm^{-1}), —C=C— (high intensity at 1618 cm^{-1}), —O—H (3436 cm^{-1}) corresponds to RGO. The peak at 2082 cm^{-1} designates the presence of cyano from Prussian blue. XRD and FTIR analysis confirms the existence of magnetite, prussian blue, reduced graphene oxide in aerogel.

SEM analysis of aerogel revealed the surface morphology. Fig. 3(a and b) with different magnification displayed a well-defined and interconnected self-assembled porous network with hierarchical pores. The walls of these micropores contain dispersed PB and magnetite over wrinkled graphene sheets which can be seen from Fig. 3c (HR-TEM image). It can be observed that Fe_3O_4 nanoparticles and PB anchored over the surface of single graphene sheets which reduces their aggregation as shown in Figure S1 (Jang et al., 2015). The SAED (selected area electron diffraction) pattern corresponds to the crystallinity of anchored Prussian blue-coated Fe_3O_4 nanoparticles as shown in Fig. 3d.

MPMS analysis of magnetic aerogel exhibited a typical hysteresis loop at room temperature with 16 emu/g of saturation magnetization (Figure S2). The aerogel showed supermagnetic properties resulting from zero remanence and coercivity in the

magnetization curve. Due to its magnetic property, the synthesized aerogel was quickly and effectively collected from contaminated water by using an external magnet (Figure S2b).

TGA of aerogel indicated high thermal stability as about 53% of the material remained after reaching $800\text{ }^\circ\text{C}$ (Figure S3). The initial weight loss is loss of moisture while the further weight loss might be due to decomposition of organic material.

Fig. 4a shows the detailed survey XPS spectrum of aerogel which exhibits the presence of iron, carbon, nitrogen, and oxygen. To evaluate the electronic states of different elements, detailed analysis was done. Peak fitting of C1s gave different peaks at 288.9, 287.8, 286.5, 285.7 and 284.5 eV which corresponded to O—C=O , $\text{—C}\equiv\text{N—}$, —C=O , —C—O and C=C/C—C . The intensity of the peak for C=C/C—C is high, which indicates the reduction of graphene oxide. The peak at 285.7 eV (cyano group of $[\text{Fe}(\text{CN})_6]^{4-}$) revealed the existence of PB in aerogel. The Fe 2p peak profile shows two peaks which are at 711.3 and 724.9 eV corresponding to iron of Fe_3O_4 while one peak at 708.3 eV related to that of prussian blue (Chen et al., 2012). The N1s peak fitting showed three components at 399.2, 398 and 397 eV, which approves the presence of $\text{—C}\equiv\text{N}$ ($[\text{Fe}(\text{CN})_6]^{4-}$) in composites. XPS analysis gave proof for the existence of magnetite, PB and RGO in the synthesized aerogel.

For adsorption of Cs ion, the surface area of adsorbent plays an important role and BET surface area analysis of aero-

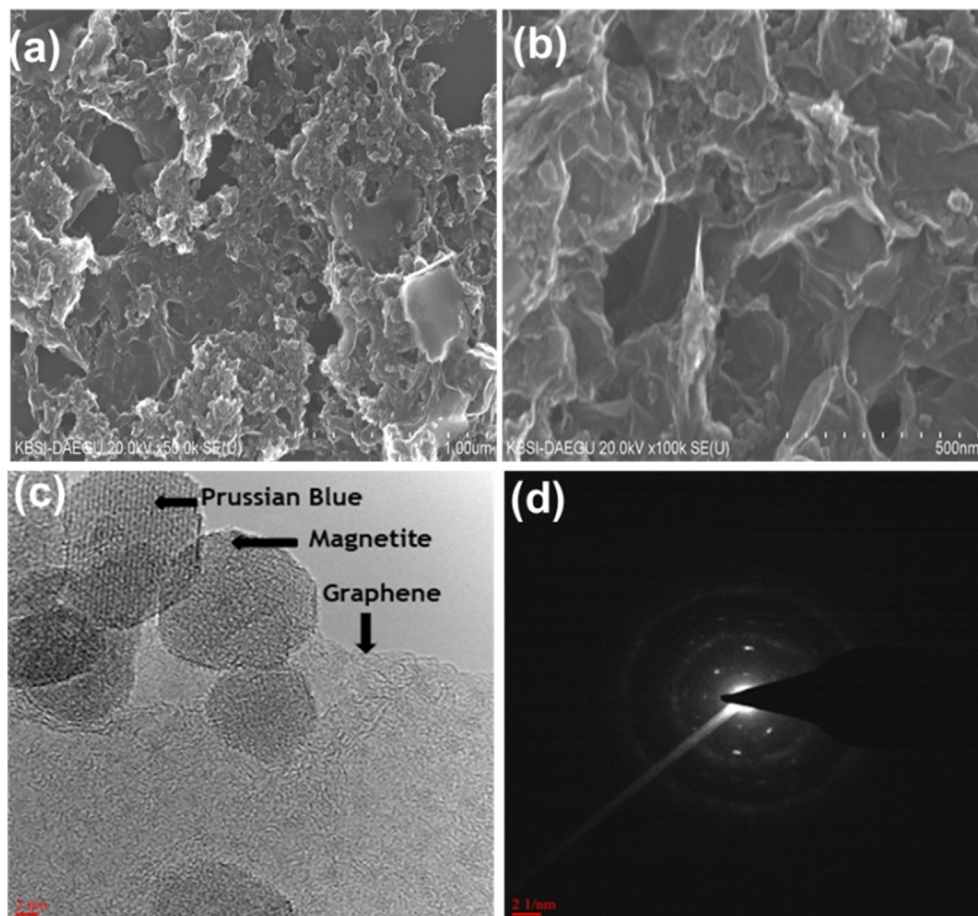


Fig. 3 SEM images of 3D-MPBRGO with different magnification (a, b) and TEM image with SAED pattern (c, d).

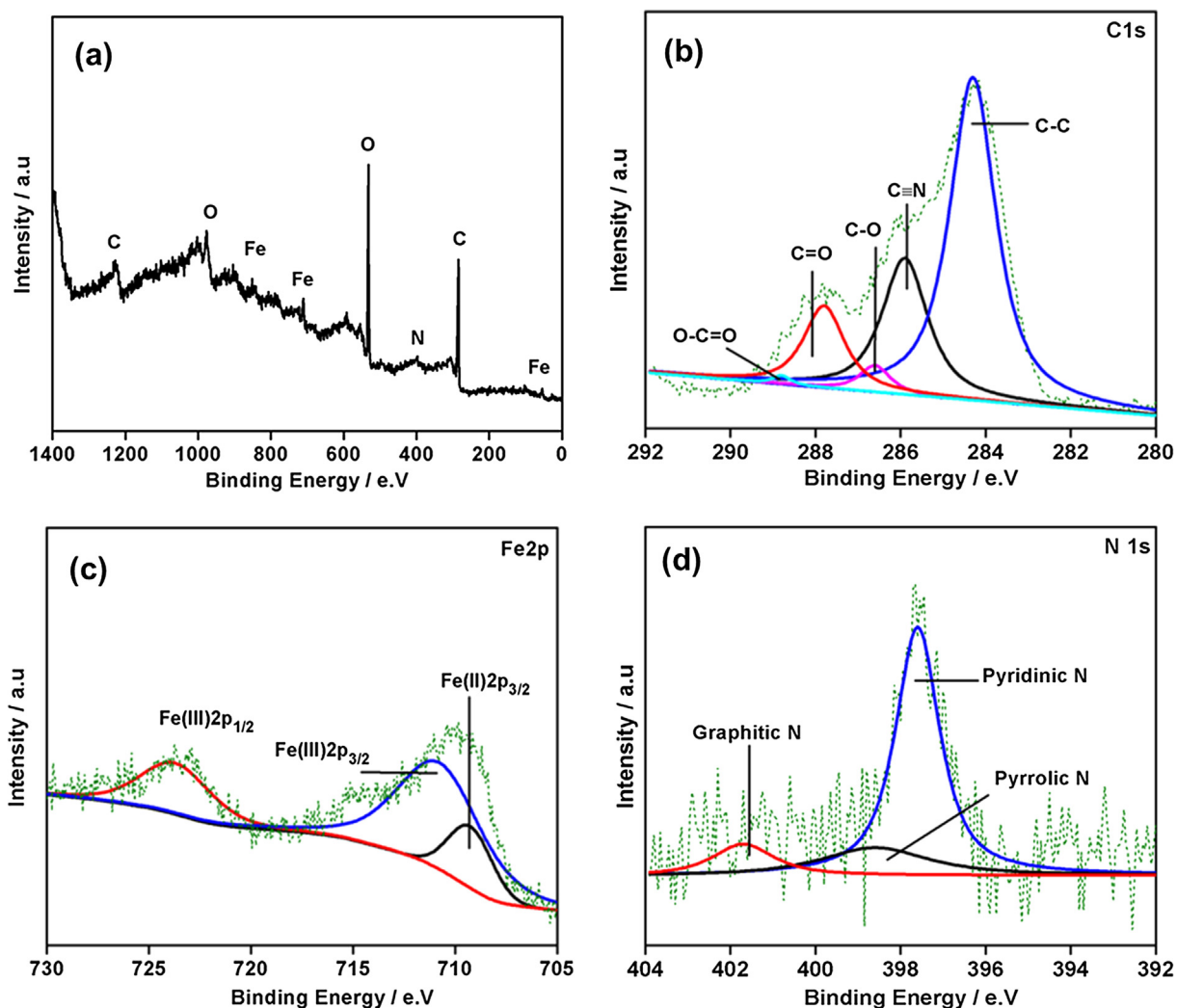


Fig. 4 (a) XPS detailed survey of aerogel (b) C1s (c) Fe2p and (d) N1s peak profile.

gel confirmed high adsorptive surface area ($402.62 \text{ m}^2/\text{g}$) of aerogel (Figure S4 and Table S1). The surface area of the aerogel is more than the previously published articles regarding cesium adsorption. The average pore diameter of aerogel was 4.34 nm , which approves that the material was mesoporous in nature that enhanced the transmission of cesium ions via the aerogel, and perform as an effective adsorbent. The HR-TEM EDX shows composition of elements related to the existence of cesium ions on the aerogel's surface after the removal of Cs via adsorption from aqueous solution (Fig. 5b).

HR-TEM analysis revealed that uniform dispersal of nitrogen (from Prussian blue) and iron (from magnetite/PB) was observed over the nanomaterial (Figure S5 and S6). A comprehensive assessment of Cs dispersal exhibited that it was found more above the surface where N was present in large quantity. These results give strong evidence that Cs ion adsorption was assisted by the uniform dispersal of PB on aerogel.

3.2. Adsorption studies

In this paper, easily fabricated aerogel displayed an excellent adsorption capability of 3.64 mmol/g for cesium ions which

is higher than that of the previous work regarding cesium ion removal by graphene based nanomaterial (Sun et al., 2013).

(Fig. 6). The increased adsorption efficiency of aerogel was ascribed to high surface area of adsorbent and separation of RGO sheets by incorporating magnetite and PB via self-assembled technique. Effect of pH is very significant factor in the adsorption therefore the optimized pH for the process on aerogel was found to be 7. Neither the acidic nor the basic medium is suitable for PB due to its dissolution in acidic while it decompose in alkaline medium. The temperature effect was also optimized for adsorption phenomena and found to be $30 \text{ }^\circ\text{C}$ (Fig. 6b).

3.2.1. Adsorption isotherms

To determine the maximum adsorption capacity of adsorbent for cesium ion removal and understanding the adsorption mechanism it is essential to know the equilibrium dispersal of cesium ion between adsorbent and the adsorbate. Langmuir, Freundlich, and Tempkin isotherms models were used for experimental data. A nonlinear regression method was applied by using Langmuir, Freundlich, and Tempkin models

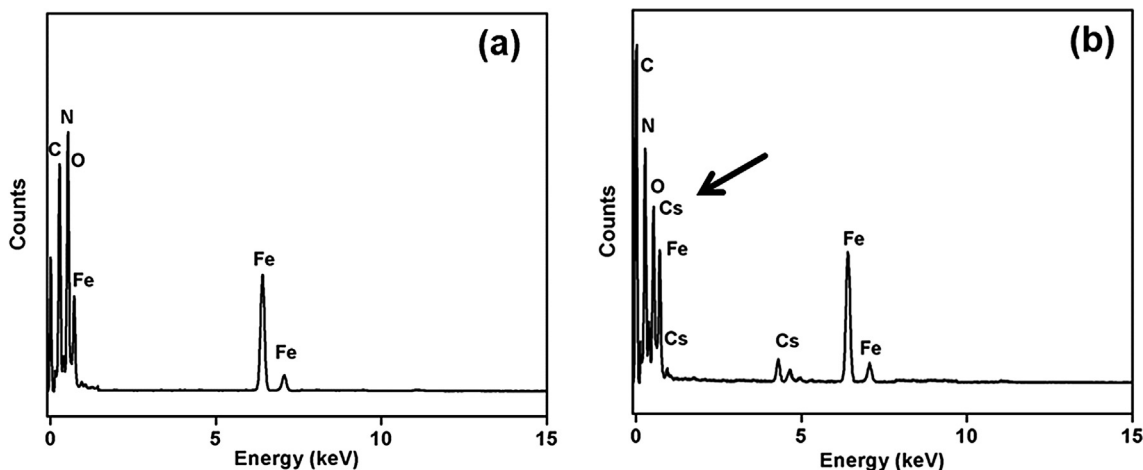


Fig. 5 HR-TEM EDX of Cs over aerogel (a) before and (b) after adsorption process.

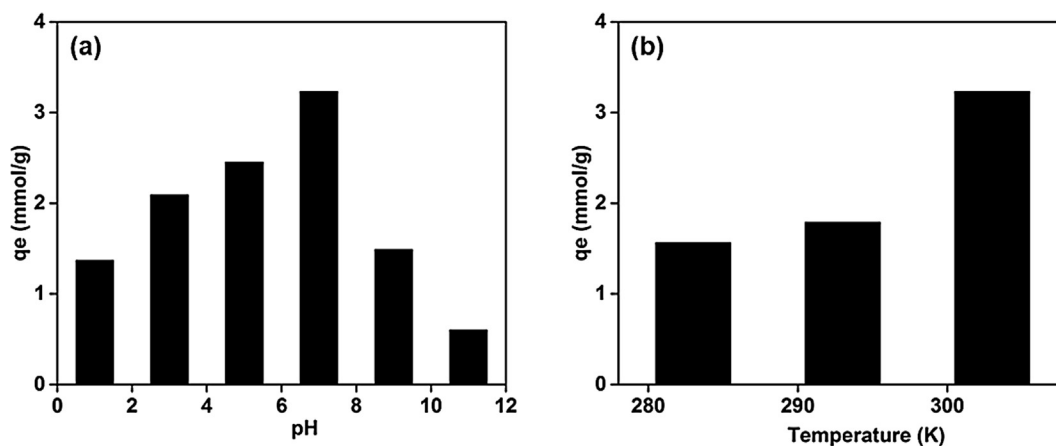


Fig. 6 Cesium removal by aerogel (a) pH effect on cesium removal (b) temperature effect on cesium removal. (Initial concentration of cesium-50 mmol).

(Eqs. (3)–(5)) respectively for determination of adsorption capacity (Langmuir, 1916; Freundlich, 1906; Tempkin and Pyzhev, 1940).

$$q_e = \frac{q_m K_L C_e}{1 + K_L C_e} \quad (3)$$

$$q_e = K_F C_e^{(1/n)} \quad (4)$$

$$q_e = \frac{RT}{b_T \ln(A_T C_e)} \quad (5)$$

The adsorption capability of adsorbent at equilibrium is q_e (mg/g), q_m (mg/g) is the adsorption capability of monolayer, C_e is cesium concentration at equilibrium, K_L (L/mg), K_F (mg/g), R (8.314 J/mol/K) is gas constant while the remaining are isotherm constants. The chi-squared (χ^2) and average percentage errors (APE) equations were used for the fitness of isotherm equations which are as follows (Ho and Wang, 2004).

$$\chi^2 = \frac{\sum (q_{e,calc} - q_{e,exp})^2}{q_{e,exp}} \quad (6)$$

$$APE = 100/n \sum \left| \frac{(q_{e,calc} - q_{e,exp})}{q_{e,exp}} \right| \quad (7)$$

where $q_{e,exp}$, $q_{e,calc}$ are the experimental and calculated values respectively while n , is number of observations. Nonlinear regression method was used for determination of non-linearized coefficients. Comparing the non-linearized isotherms in terms of correlation coefficient (r^2) and χ^2 are given in Table 1 (Figure S7).

Table 1 Comparison of adsorption isotherm models for Cs adsorption on aerogel.

Isotherm models	Isotherm parameters	χ^2	r^2
Langmuir	$q_m = 3.64$ mmol/g, $K_L = 0.11$ L/mg	0.10	0.985
Freundlich	$K_F = 0.97$ mmol/g, $n = 3.55$	0.91	0.873
Tempkin	$A = 1.96$, $B = 1667$	0.29	0.959

Table 2 Comparison of adsorbents in terms of surface area and Cs adsorption capability.

Type of adsorbent	Specific surface area (m ² /g)	q _m (mmol/g)/ (mg/g)	Refs.
3D-MPBRGO	402.62	3.64/484.12	This study
PANI@GO	140.8	1.39/184.87	14
PB/Fe ₃ O ₄ /GO	152.91	0.41/55	9
3D-PB/RGOF	43.07	0.14/18.62	12

The obtained results at equilibrium follows Langmuir isotherm with r² value of 0.98 as compared to Freundlich and Tempkin isotherms. The q_m and K_a values for cesium ion adsorption of aerogel are 484.12 mg/g and 0.1 L/mg respectively. Table 2 displayed comparison of different graphene based adsorbents with this work. The favorability of adsorption can be endorsed via Eq. (8) which was used to determine separation factor R_L where it exhibited the isotherm shape. C₀ is the cesium concentration initially while the Langmuir constant is K_a. The value of R_L in between 0 and 1 indicated the favorable interface.

$$R_L = \frac{1}{1 + K_a C_0} \quad (8)$$

3.2.2. Adsorption kinetic study

Two kinetic models (pseudo 1st and 2nd order) used for adsorption of cesium ion which are shown as Eqs. (9) and (10). Where q_t and q_e are the cesium concentration adsorption at time t (min) and equilibrium respectively. Rate constants (min⁻¹) are k₁ and k₂ for 1st and 2nd order respectively.

$$q_t = q_e(1 - e^{-k_1 t}) \quad (9)$$

$$q_t = \frac{k_2 q_e t}{1 + k_2 q_e t} \quad (10)$$

Fig. 7 clearly displays that adsorption of cesium reaches equilibrium (cesium ion, 484.12 mg/g) in 24 h. The correlation coefficient obtained from the pseudo second order (r² = 0.988)

was higher than that of the first order (r² = 0.985), signifying that adsorption of cesium on aerogel is a chemisorption.

3.3. Thermodynamic analysis

Thermodynamic parameters (Gibbs free energy change (ΔG°), entropy (ΔS°) and enthalpy (ΔH°)) applied to determine the nature and feasibility of the process of adsorption. The ΔG° is related to the equilibrium constant (K_c = 1000 q_e/C_e) by following equation (Debnath et al., 2014).

$$\Delta G^\circ = -RT \ln K_c \quad (11)$$

Eq. (12) shows that the change in entropy can be related that of Gibbs free at constant temperature according to thermodynamics.

$$\Delta G^\circ = \Delta H^\circ - T\Delta S^\circ \quad (12)$$

The ΔH° and ΔS° determined by taking slope and intercept of the linear plots of ΔG° with respect to temperature. The negative sign with the ΔG° value increases with increase in temperature, which approves practicality and naturalness of cesium ion adsorption on aerogel. The negative value of ΔH° (-7.67 kJ/mol) shows the exothermic nature of process while positive value of ΔS° (0.101 kJ/mol) also refer to an increase in cesium ions from solution at interface which is probably due to the release of molecules of water.

4. Conclusions

The 3D-MPBRGO (novel) aerogel was effectively prepared for removal of cesium ion selectively from radioactive waste water. Self assembled RGO sheets with high surface area resulted in increased cesium ion adsorption. The adsorption process was exothermic, feasible and spontaneous on the basis of thermodynamic analysis. The experimental data followed Langmuir isotherm based on nonlinear regression. Inclusively the aerogel was found to be an effective adsorbent for selective removal of cesium from radioactive aqueous solution waste, and can be simply recovered after adsorption process by applying an external magnet which increases its applicability on commercial level.

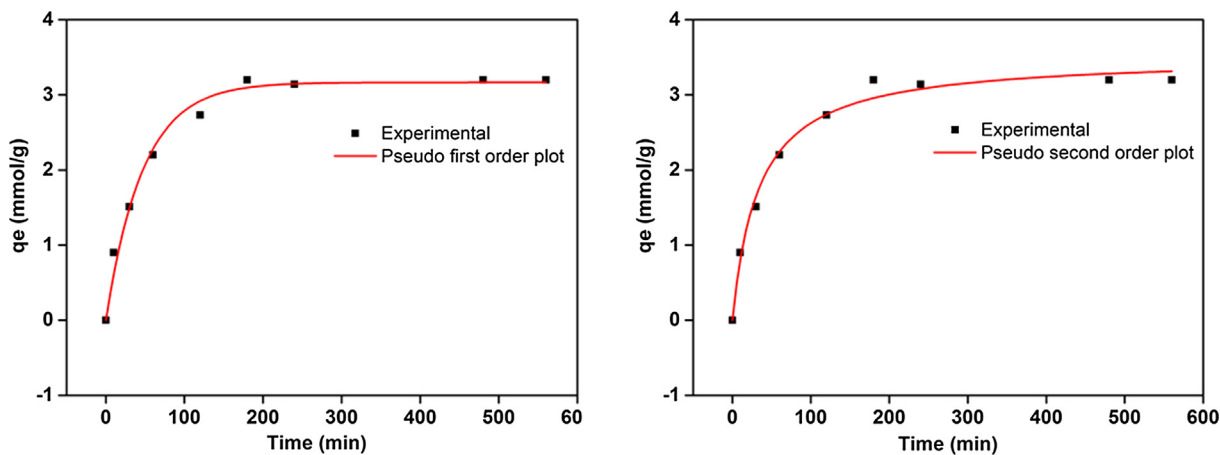


Fig. 7 Adsorption kinetics study. Pseudo (a) First and (b) Second order.

Acknowledgements

This research was supported by the HEC, Pakistan (7737/KP K/NRPU/R&D/HEC/2017).

Appendix A. Supplementary data

Supplementary data to this article can be found online at <https://doi.org/10.1016/j.arabjc.2019.08.009>.

References

- Chen, L., Wang, X., Zhang, X., Zhang, H., 2012. 3D porous and redox-active Prussian blue-in-graphene aerogels for highly efficient electrochemical detection of H₂O₂. *J. Mater. Chem.* 22, 22090–22096.
- Cong, H.P., He, J.J., Lu, Y., Yu, S.H., 2010. Water-soluble magnetic-functionalized reduced graphene oxide sheets: in situ synthesis and magnetic resonance imaging applications. *Small* 6, 169–173.
- Debnath, S., Maity, A., Pillay, K., 2014. Magnetic chitosan-GO nanocomposite: synthesis, characterization and batch adsorber design for Cr(VI) removal. *J. Environ. Chem. Eng.* 2, 963–973.
- Freundlich, H., 1906. Over the adsorption in solution. *J. Phys. Chem.* 57, 51–85.
- Ho, Y.S., Wang, C.C., 2004. Pseudo-isotherms for the sorption of cadmium ion onto tree fern. *Process Biochem.* 39, 759–763.
- Jang, S.-C., Haldorai, Y., Lee, G.-W., Hwang, S.-K., Han, Y.-K., Roh, C., Huh, Y.S., 2015. Porous three-dimensional graphene foam/Prussian blue composite for efficient removal of radioactive ¹³⁷Cs. *Sci. Rep.* 5, 17510.
- Langmuir, I., 1916. The constitution and fundamental properties of solids and liquids. Part I. Solids. *J. Am. Chem. Soc.* 38, 2221–2295.
- Liu, X., Chen, G.R., Lee, D.J., Kawamoto, T., Tanaka, H., Chen, M. L., Luo, Y.K., 2014. Adsorption removal of cesium from drinking waters: a mini review on use of biosorbents and other adsorbents. *Bioresour. Technol.* 160, 142–149.
- Massart, R., 1981. Preparation of aqueous magnetic liquids in alkaline and acidic media. *IEEE Trans. Magn.* 17, 1247–1248.
- Romanchuk, A.Y., Slesarev, A.S., Kalmykov, S.N., Kosynkin, D.V., Tour, J.M., 2013. Graphene oxide for effective radionuclide removal. *Phys. Chem. Chem. Phys.* 15, 2321–2327.
- Seema, H., Kemp, K.C., Le, N.H., Park, S., Chandra, V., Lee, J.W., 2014. Highly selective CO₂ capture by S-doped microporous carbon materials. *Carbon* 66, 320–326.
- Sun, H.M., Cao, L.Y., Lu, L.H., 2011. Magnetite/reduced graphene oxide nanocomposites: one step solvothermal synthesis and use as a novel platform for removal of dye pollutants. *Nano Res.* 4, 550–562.
- Sun, Y., Shao, D., Yang, S., Wang, X., 2013. Highly efficient enrichment of radionuclides on graphene oxide-supported polyaniline. *Environ. Sci. Technol.* 47, 9904–9910.
- Tempkin, M., Pyzhev, V., 1940. Kinetics of ammonia synthesis on promoted iron catalyst. *Acta Phys. Chim. USSR.* 12, 327–356.
- Torad, N.L., Hu, M., Imura, M., Naito, M., Yamauchi, Y., 2012. Large Cs adsorption capability of nanostructured Prussian blue particles with high accessible surface areas. *J. Mater. Chem.* 22, 18261–18267.
- Yang, H., Sun, L., Zhai, J., Li, H., Zhao, Y., Yu, H., 2014. In situ controllable synthesis of magnetic Prussian blue/graphene oxide nanocomposites for removal of radioactive cesium in water. *J. Mater. Chem. A* 2, 326–332.
- Yantasee, W., Warner, C.L., Sangvanich, T., Addleman, R.S., Carter, T.G., Wiacek, R.J., Fryxell, G.E., Timchalk, C., Warner, M.G., 2007. Removal of heavy metals from aqueous systems with thiol functionalized superparamagnetic nanoparticles. *Environ. Sci. Technol.* 41, 5114–5119.
- Yavuz, C.T., Mayo, J.T., Yu, W.W., Prakash, A., Falkner, J.C., Yean, S., Cong, L., Shipley, H.J., Kan, A., Tomson, M., Natelson, D., Colvin, V.L., 2006. Low-field magnetic separation of monodisperse Fe₃O₄ nanocrystals. *Science* 314, 964–967.
- Zhang, Y., Chen, B., Zhang, L.M., Huang, J., Chen, F.H., Yang, Z.P., Yao, J.L., Zhang, Z.J., 2013. Controlled assembly of Fe₃O₄ magnetic nanoparticles on graphene oxide. *Nanoscale* 3, 1446–1450.